ELASTO-VISCOPLASTIC PROPERTIES OF AA2017 ALUMINIUM ALLOY

ANDRZEJ AMBROZIAK, PAWEŁ KŁOSOWSKI AND ŁUKASZ PYRZOWSKI

Department of Structural Mechanics and Bridge Structures,
Faculty of Civil and Environmental Engineering,
Gdansk University of Technology,
Narutowicza 11/12, 80-233 Gdansk, Poland
{ambrozan, klosow, lpyrzow}@pg.gda.pl

Abstract: This paper describes a procedure for the identification of material parameters for the elasto-viscoplastic Bodner-Partom model. A set of viscoplastic parameters is identified for AA2017 aluminium alloy. The evaluation of material parameters for the Bodner-Partom constitutive equations is carried out using tensile tests. Numerical simulations of material behaviour during constant strain-rate tests are compared with direct uniaxial tensile experiments. A review of the models applied to concisely describe aluminium alloy is also given.

Keywords: AA2017, viscoplasticity, Bodner-Partom, tensile tests

1. Introduction

Aluminium alloy is commonly used in the aircraft industry, building and construction industry, electricity, packaging, transportation, *etc.* It is an alloy of intermediate strength and good ductility. The main alloying elements are copper, magnesium, zinc, silicon, manganese and lithium. In the case of AA2017 aluminium alloy, the main alloying element is copper, see *e.g.* [1].

The selection of constitutive models is one of the most important problems, which is considered before other aspects of structural analysis. Different approaches to constitutive modelling of the behaviour of aluminium alloys (such as nonlinear elastic, viscoplastic, viscoelastic) can be considered. Very often, the undertaken approach depends not only on the material properties, but also on the type of loading under consideration.

In 1943, Ramberg and Osgood [2] proposed an elasto-plastic model for the description of the behaviour of aluminium alloy, stainless steel and carbon steel. This model is used in many practical engineering applications. Kuruppu *et al.* [3]

presented an extension of the Ramaswamy, Stouffer, and Laflen unified elastic-viscoplastic theory to the description of the strain-rate insensitive 7050-T7451 aluminium alloy. Kowalewski *et al.* [4] described the creep behaviour of aluminium alloy at 150°C by constitutive equations using a hyperbolic sine function of stress. Two mechanisms were identified by Kowalewski *et al.* [4]: creep-constrained cavitation and the ageing of particulate microstructure. Gelin and Ghouati [5] applied the inverse identification method to identify the viscoplastic parameters of aluminium alloy. Santhanam [6] used an elastic-viscoplastic constitutive model with an isotropic internal variable to describe the behaviour of aluminium alloy during hot-forming. Zhao and Lee [7] described simulation springback. Material parameters of 6022-T4 aluminium sheets were identified by an inverse method. Lauro *et al.* [8] presented an identification procedure for the damage parameters for aluminium. An inverse method consists in correlating the experimental and numerical measurements with a tensile test on a notched specimen. Omersphanic *et al.* [9] identified material parameters for high-strength steel alloys ZSte340 and DP600 and for AA5182 aluminium alloy. Martínez *et al.* [10] described the constitutive model for low temperatures and the plastic strain rates for the cold forming of 2117-T4 alloy. The parameters of the Hansel-Spittel and hyperboloid-type models were also identified. Diot *et al.* [11] described the rheological characterisation of Al-Mg alloy at strain rates from 0.01 to $10\,\mathrm{s}^{-1}$, at temperatures from 423 to 673 K. Omerspahic [12] determines damage propagation in ZSte340 high-strength steel alloy and in AA5182 aluminium alloy sheets. The approach for the identification of the isotropic material damage parameters is based on continuous uniaxial tensile loading and unloading of metal sheets. A global optimization technique was used by Majak *et al.* [13] to determine the material parameters of AA6181-T4 aluminium alloy sheets. Chaparro *et al.* [14] employed a genetic algorithm and a gradient-based algorithm to determine the material parameters of EN AW-5754 aluminium alloy. Bauffioux *et al.* [15] developed an inverse method for adjusting the material parameters in single point incremental forming. In [15], AA3103-O aluminium alloy is examined. Zhang *et al.* [16] described the material behaviour of 5083 aluminium alloy at high temperatures (150, 240 and 300°C). Swift hardening law was used to describe the visco-plastic behaviour of the alloy.

It should be noted that the particularities of the process for the determination of the material parameters can vary in each case. This process is sensitive to the initial values of the parameters. Thus, it is possible to obtain different values of the parameters for the same material. These different set of parameters can exactly describe behaviour of aluminium alloy.

2. Laboratory tests

We carried out experiments with AA2017 aluminium alloy at room temperature, using five different values for the constant strain rates: $\dot{\varepsilon} = 1 \cdot 10^{-4}\,\mathrm{s}^{-1}$, $\dot{\varepsilon} = 5 \cdot 10^{-4}\,\mathrm{s}^{-1}$, $\dot{\varepsilon} = 1 \cdot 10^{-3}\,\mathrm{s}^{-1}$, $\dot{\varepsilon} = 1 \cdot 5^{-3}\,\mathrm{s}^{-1}$, $\dot{\varepsilon} = 1 \cdot 10^{-2}\,\mathrm{s}^{-1}$. Two types of spec-

imens were examined – one cut along and one across the rolling direction of the sheet. The specimens were 15 cm long, 1.2 cm wide, and 0.1 cm thick. All uniaxial experiments were performed using a Zwick/Roell Z020 Universal Testing Machine equipped with an extensometer. The clamp spacing was set to 7.5 cm, whereas the gauge length was 4.0 cm (see Figure 1).
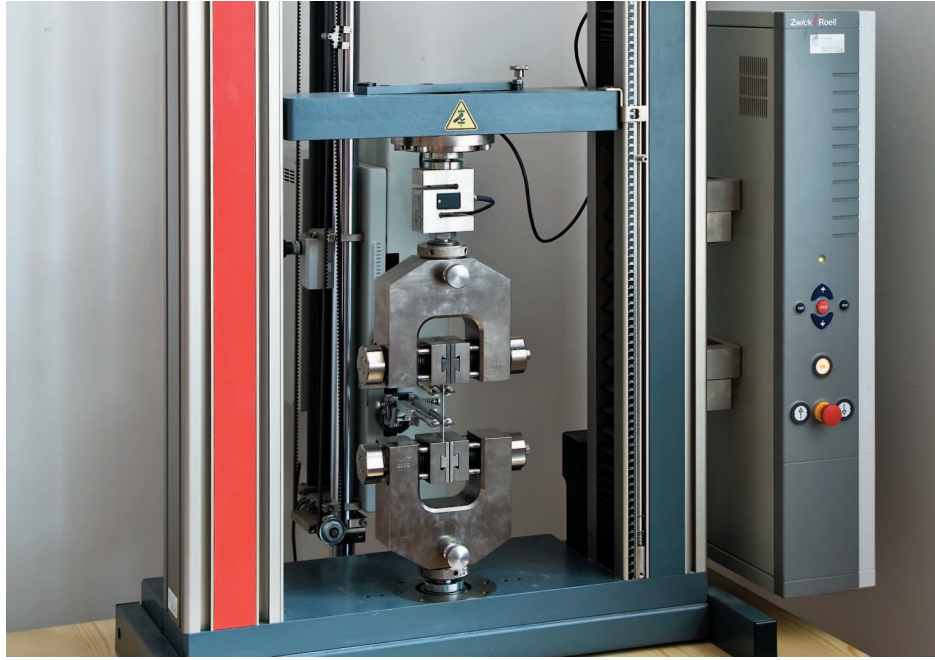

Figure 1. Experimental stand

3. Determination of elastic material parameters

First, we transformed the displacement-force data obtained from the measurements to obtain the strain-stress relationship. The engineering strain and stress were used.

Initially, the elastic tensile modulus E was determined for the specimens of AA2017, using linear approximation (column 2 of Table 1 and Table 2). The elastic tensile modulus in the strain range of $\varepsilon \in \langle 0, 0.003 \rangle$ was specified.

Subsequently, the inelastic strain ε^I was calculated as:

$$\varepsilon^I = \varepsilon - \frac{\sigma}{E} \tag{1}$$

where ε is the total strain and σ is the stress. It was assumed that when the inelastic strain exceeds zero, the yield limit value is reached (see Table 1 and Table 2).

The obtained results indicate that the magnitude of viscous effects is small, nevertheless, an elasto-viscoplastic constitutive model can be applied, particularly

Table 1. Values of the elasticity modulus and the yield limit for the specimen cut across the rolling direction of the sheet

$\dot{\varepsilon}$ [s^{-1}]	E [MPa]	σ_γ [MPa]	$\overline{E}$ [MPa] mean values	$\overline{\sigma}_\gamma$ [MPa] mean values
0.0001	67 525	228.0	67 525 ± 0	228.0 ± 0
0.0005	68 546	227.4	68 277 ± 380	229.3 ± 2.7
	68 007	231.2		
0.001	68 590	230.6	69 737 ± 1621	232.2 ± 2.3
	70 883	233.9		
0.005	69 045	238.2	69 105 ± 84	238.3 ± 0.2
	69 164	238.4		
0.01	69 837	235.5	69 226 ± 864	233.0 ± 3.5
	68 615	230.5		

Table 2. Values of the elasticity modulus and the yield limit for the specimen cut along the rolling direction of the sheet

| $\dot{\varepsilon}$ [s^{-1}]	E [MPa]	σ_γ [MPa]	$\overline{E}$ [MPa] mean values	$\overline{\sigma}_\gamma$ [MPa] mean values
0.0001	69 812	251.66	69 812 ± 0	251.7 ± 0
0.0005	70 666	249.18	70 704 ± 54	251.8 ± 3.7
	70 743	254.38		
0.001	71 000	254.5	71 258 ± 364	255.4 ± 1.3
	71 516	256.4		
0.005	71 903	254.8	70 995 ± 1284	253.7 ± 1.5
	70 087	252.7		
0.01	71 229	257.9	70 754 ± 671	256.9 ± 1.3
	70 279	256.0		

so in the case of either long-lasting or very rapid loads. On the other hand, certain authors deemed viscous effects negligible and, therefore, applied elasto-plastic constitutive models to describe aluminium alloys. Although the rolling direction was observed to have a small influence on the yield limit, the authors of the present paper have decided to apply isotropic modelling. On the basis of the mean values of the yield limit $\overline{\sigma}_\gamma$, the elastic tensile modulus $\overline{E}$ was determined (see Table 3). A graphical visualization of the distribution of the mean yield limit is shown in Figure 2.

4. Description of the constitutive model

From a wide range of available viscoplastic constitutive models, the Bodner-Partom model [17] was chosen. This model belongs to a group of isotropic constitutive models, which are used to describe the elasto-viscoplastic behaviour

Table 3. Mean values of the elasticity modulus and the yield limit

$\dot{\varepsilon}$ [s^{-1}]	$\overline{\sigma}_\gamma$ [MPa]	$\overline{E}$ [MPa]
0.0001	239.8	
0.0005	240.5	
0.001	243.8	69 700
0.005	246.0	
0.01	245.0	
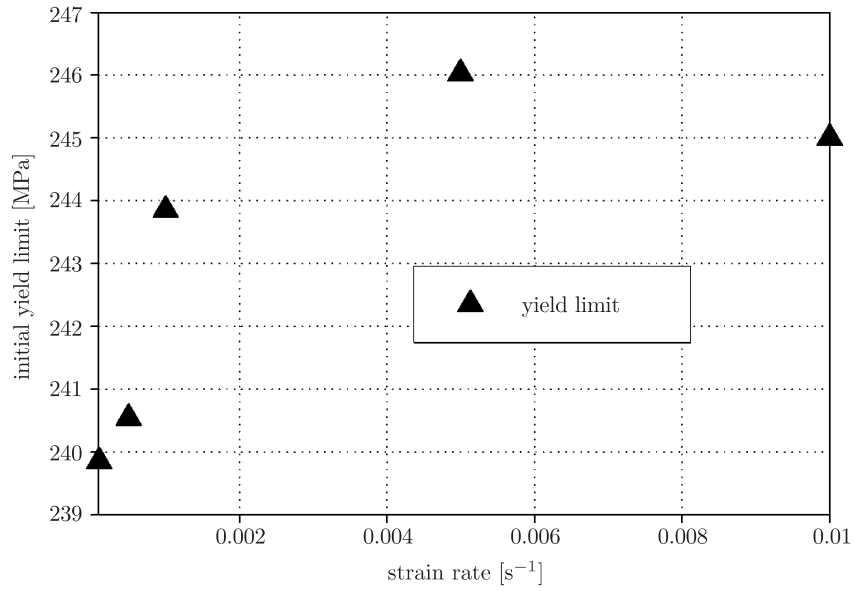
Figure 2. Conventional yield limit – on a linear scale

of materials for small inelastic deformations and small strain rates (since the model is additive), see *e.g.* [18].

First, an additive decomposition of the total strain rate $\dot{\boldsymbol{\varepsilon}}$ (for small strain rates $\dot{\varepsilon} < 0.1\,\text{s}^{-1}$) was assumed:

$$\dot{\boldsymbol{\varepsilon}} = \dot{\boldsymbol{\varepsilon}}^E + \dot{\boldsymbol{\varepsilon}}^I \tag{2}$$

where $\dot{\boldsymbol{\varepsilon}}^E$ and $\dot{\boldsymbol{\varepsilon}}^I$ are the elastic and inelastic strain rate, respectively. The relation between the stress rate $\dot{\boldsymbol{\sigma}}$ and the strain rate $\dot{\boldsymbol{\varepsilon}}^E$, for the assumed isotropic material, was defined as:

$$\dot{\boldsymbol{\sigma}} = \boldsymbol{D} \cdot \dot{\boldsymbol{\varepsilon}}^E = \boldsymbol{D} \cdot (\dot{\boldsymbol{\varepsilon}} - \dot{\boldsymbol{\varepsilon}}^I) \tag{3}$$

where $\boldsymbol{D}$ is the standard elasticity tensor.

In the Bodner-Partom model [17], the inelastic strain rate $\dot{\boldsymbol{\varepsilon}}^I$ was given by the equation:

$$\dot{\boldsymbol{\varepsilon}}^I = \frac{3}{2}\dot{p}\frac{\boldsymbol{\sigma}'}{J(\boldsymbol{\sigma}')} \tag{4}$$

where $\dot{p}$, $\boldsymbol{\sigma}'$ and $J(\boldsymbol{\sigma}')$ are the equivalent inelastic strain rate, stress tensor deviator and its second invariant, respectively. The equivalent inelastic strain rate $\dot{p}$ was defined by the equation [17]:

$$\dot{p} = \frac{2}{\sqrt{3}} D_0 \exp\left[-\frac{1}{2}\left(\frac{\left(R + \boldsymbol{X} \cdot \frac{\boldsymbol{\sigma}}{J(\boldsymbol{\sigma})}\right)}{J(\boldsymbol{\sigma}')}\right)^{2n} \frac{n+1}{n}\right] \tag{5}$$

where the constants D_0 and n are material parameters, which represent the plastic strain rate limit and the strain-rate sensitivity parameter, respectively. If the recovery effects are neglected, the isotropic and kinematic hardening, R and $\boldsymbol{X}$, respectively, can be expressed as:

$$\dot{R} = m_1(R_1 - R)\dot{W}^I$$
$$\dot{\boldsymbol{X}} = m_2\left(\frac{3}{2} D_1 \frac{\boldsymbol{\sigma}}{J(\boldsymbol{\sigma})} - \boldsymbol{X}\right)\dot{W}^I \tag{6}$$

where m_1 is the hardening rate coefficient for isotropic hardening; R_1 is the limiting value for isotropic hardening; m_2 is the hardening rate coefficient for kinematic hardening; and D_1 is the limiting value for kinematic hardening.

The initial value of isotropic hardening was $R(t=0) = R_0$, which should be regarded as a material parameter. The inelastic work rate $\dot{W}^I$ in Equation (6), was calculated from the equation:

$$\dot{W}^I = \boldsymbol{\sigma} \cdot \dot{\boldsymbol{\varepsilon}}^I \tag{7}$$

In the described model, seven inelastic parameters must be determined: n, D_0, D_1, R_0, R_1, m_1, m_2 and, additionally, two elastic constants E, ν must be known. On the basis of laboratory tests, all material parameters were determined. Least-squares regression was performed using the commercial package SigmaPlot. The curve filter implemented in SigmaPlot uses the Marquardt-Levenberg algorithm [19] to find the coefficients of the independent variables that give the best fit between the equation and the data.

5. Determination of inelastic material parameters

It was assumed that the investigated material has elasto-viscoplastic properties, which are well-described by the Bodner-Partom model. At the beginning of the identification process for the Bodner-Partom model, the parameter $D_0 = 10^4\,\mathrm{s}^{-1}$ (for quasi-static analysis, where the strain rate does not exceed $10\,\mathrm{s}^{-1}$) was arbitrarily chosen.

In addition, it was observed that for the initial value of the hardening, $R = R_0$, kinematic hardening is negligible. The determination of the parameters n and R_0 is possible on the basis of the following expression:

$$\sigma_\gamma(\dot{\varepsilon}) = \frac{R_0}{\left[\frac{2n}{n+1}\ln\left(\frac{2D_0}{\sqrt{3}\dot{\varepsilon}^I}\right)\right]^{\frac{1}{2n}}} \tag{8}$$

where σ_γ is the initial value of the yield stress. The values of the yield stress σ_γ for different strain rates are given in Table 3. The resulting function $\sigma_\gamma(\dot{\varepsilon})$ can also be
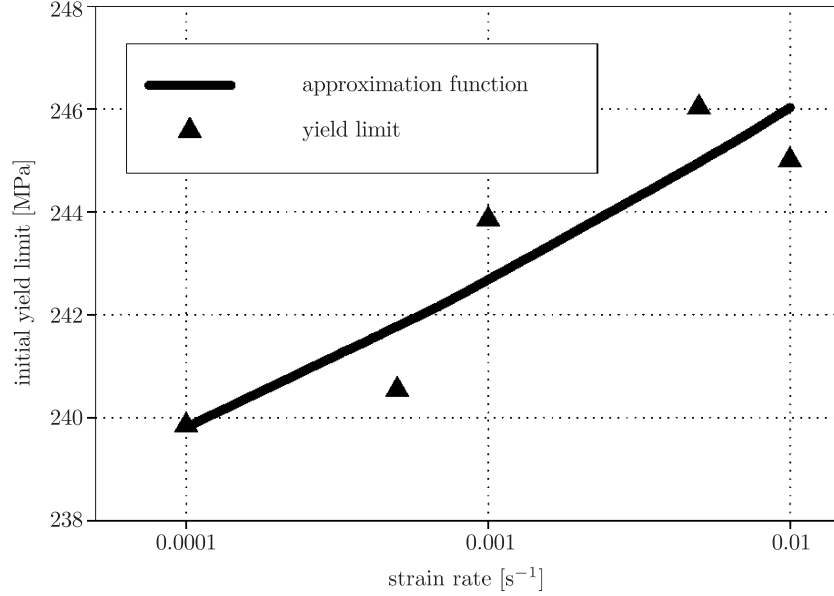
Figure 3. Yield stress expressed as a function of the strain rate, on a logarithmic scale

specified (see Figure 3). The values of the parameters $n = 5.58$ and $R_0 = 327\,\text{MPa}$ were determined.

Subsequently, the remaining inelastic parameters describing isotropic and kinematic hardening can be determined for each test. The inelastic material parameters in the strain range of $\varepsilon \in \langle 0, 0.03 \rangle$ were specified, and the relationship $\sigma(\varepsilon^I)$ was determined. In the present investigation an exponential, five-parameter approximation function (see Equation (9)) was used:

$$\sigma(\varepsilon^I) = a_1 + a_2 \left(1 - e^{-a_3 \cdot \varepsilon^I}\right) + a_4 \left(1 - e^{-a_5 \cdot \varepsilon^I}\right) \tag{9}$$

The work hardening rate function γ was calculated as:

$$\gamma = \frac{\mathrm{d}\sigma(\varepsilon^I)}{\mathrm{d}\varepsilon^I} \frac{1}{\sigma(\varepsilon^I)} \tag{10}$$

Therefore, it was possible to determine the parameters m_1 and m_2 as slopes at both extremes of the function γ (see Figure 4). For $\gamma = 0$, the stress values σ_s and σ_b were determined. Finally, the parameters D_1 and R_1 were calculated from the following equations:

$$D_1 = \frac{\sigma_b m_2}{f(\dot{\varepsilon}^I_{03})(m_2 - m_1)} - \frac{\sigma_s m_1}{f(\dot{\varepsilon}^I_3)(m_2 - m_1)} - R_0 \tag{11}$$

$$R_1 = \frac{\sigma_s m_2}{f(\dot{\varepsilon}^I_3)(m_2 - m_1)} - \frac{\sigma_b m_1}{f(\dot{\varepsilon}^I_{03})(m_2 - m_1)} - R_0 \tag{12}$$

The mean values of the parameters m_1, R_1, m_2, D_1 are shown in Table 4. The detailed procedure for the determination of the Bodner-Partom parameters was described in [20]. The parameters of the Bodner-Partom model in the case of AA2017 are given in Table 5.
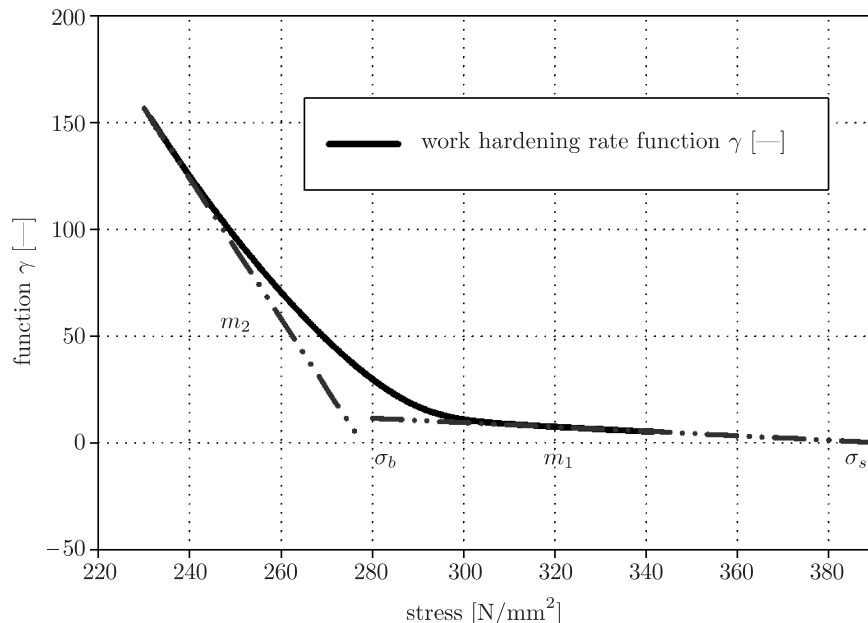
Figure 4. A graph of the function γ

Table 4. Mean values of inelastic material parameters

	mean values	across	along
m_1 [MPa^{-1}]	0.127	0.143	0.112
R_1 [MPa]	457.1	463.0	451.2
m_2 [MPa^{-1}]	4.55	4.24	4.86
D_1 [MPa]	51.5	36.9	66.2

Table 5. Elasto-viscoplastic parameters for AA2017 aluminium alloy at room temperature

E [MPa]	ν [—]	D_0 [s^{-1}]	n [—]	D_1 [MPa]	R_0 [MPa]	R_1 [MPa]	m_1 [MPa^{-1}]	m_2 [MPa^{-1}]
69 700	0.32	$1 \cdot 10^4$	5.58	51.5	327	457.1	0.127	4.55

6. Numerical simulations

Results of numerical simulations of constant strain rate tests for AA2017 aluminium alloy at different constant strain rates were compared with the results of the laboratory test performed on the specimens cut out across (see Figures 5–9) and along the rolling direction of the sheet (see Figures 10–14). The correlation coefficients calculated for each test show good agreement for both tests. The diagrams showing the stress versus strain relationship for the different strain rates are presented in Figures 15 and 16.

In paper [21], which concerns AA2017 aluminium alloy, the authors specified the elasto-viscoplastic parameters for the Chaboche model [22] (see Table 6).
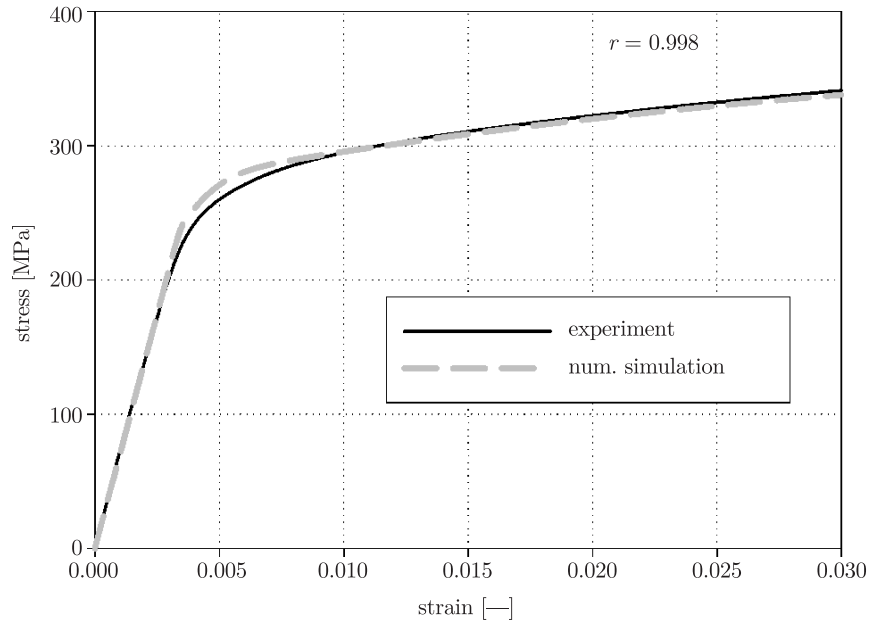
Figure 5. Results of B-P simulation of the uniaxial tension test for $\dot{\varepsilon} = 1 \cdot 10^{-4}\,\mathrm{s}^{-1}$, for the specimen cut across the rolling direction of the sheet
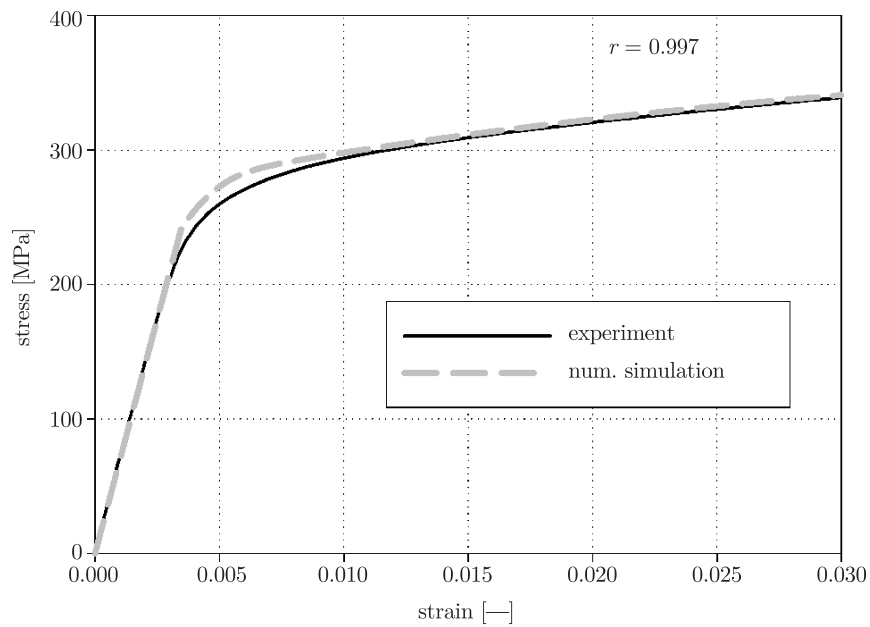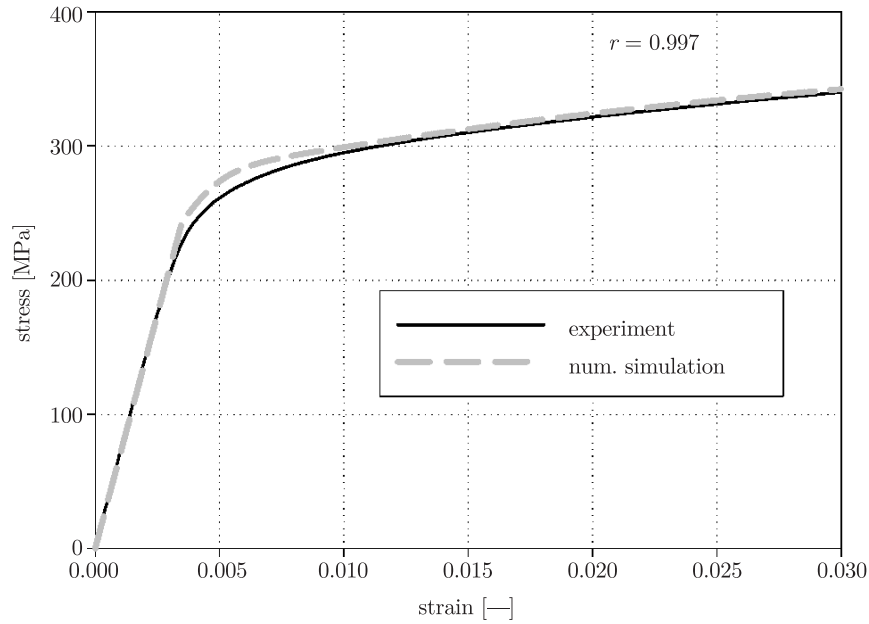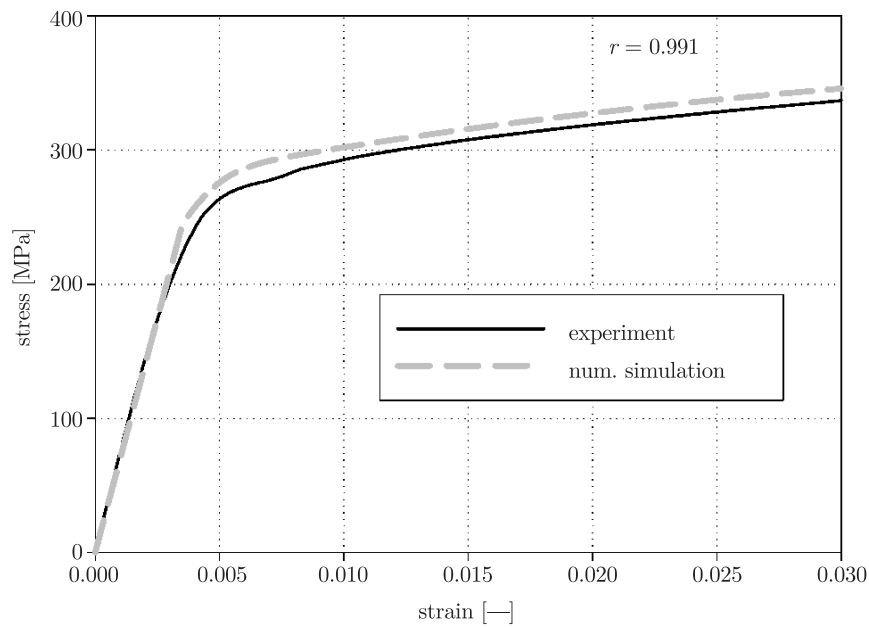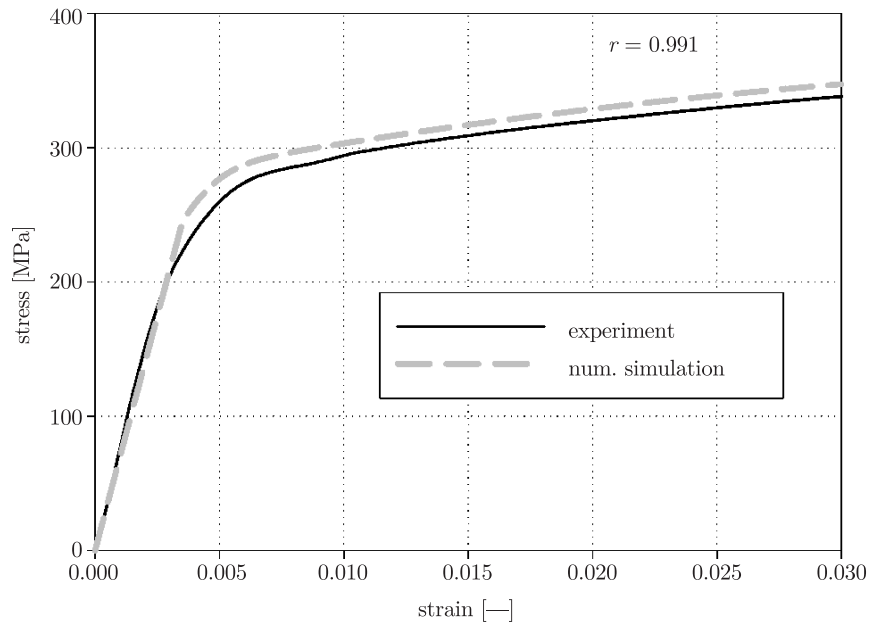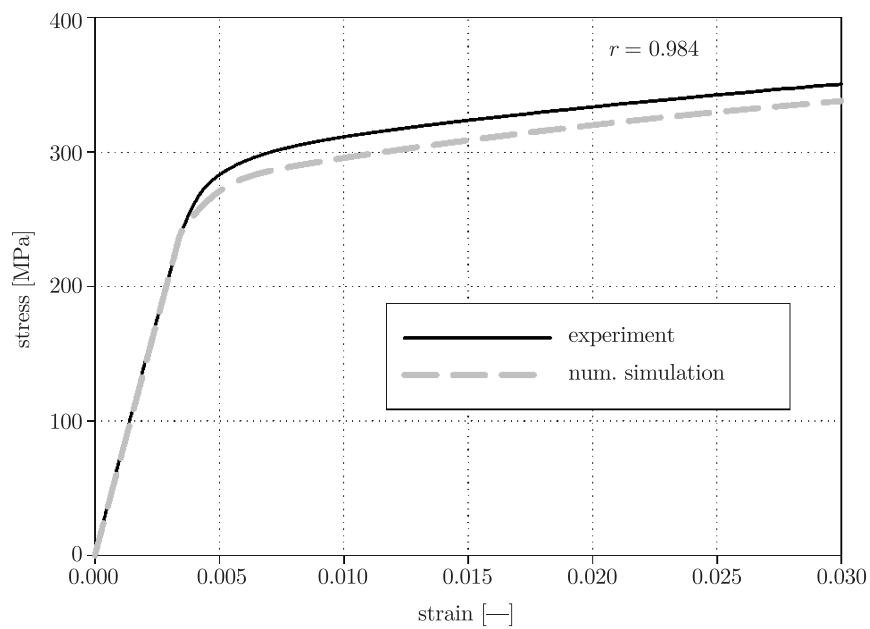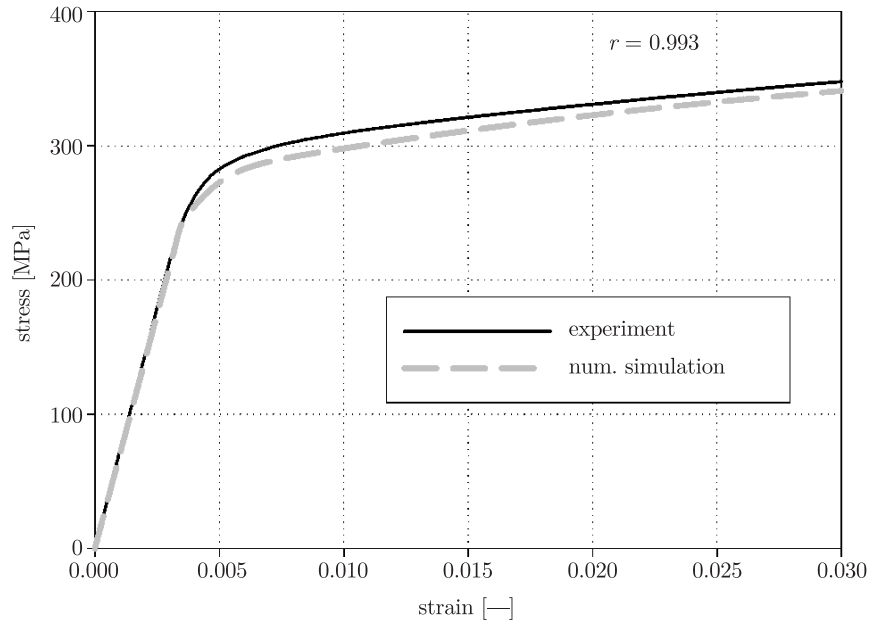

Figure 6. Results of B-P simulation of the uniaxial tension test for $\dot{\varepsilon} = 5 \cdot 10^{-4}\,\mathrm{s}^{-1}$, for the specimen cut across the rolling direction of the sheet

Figure 7. Results of B-P simulation of the uniaxial tension test for $\dot{\varepsilon} = 1 \cdot 10^{-3}\,\mathrm{s}^{-1}$,
for the specimen cut across the rolling direction of the sheet

Figure 8. Results of B-P simulation of the uniaxial tension test for $\dot{\varepsilon} = 5 \cdot 10^{-3}\,\mathrm{s}^{-1}$,
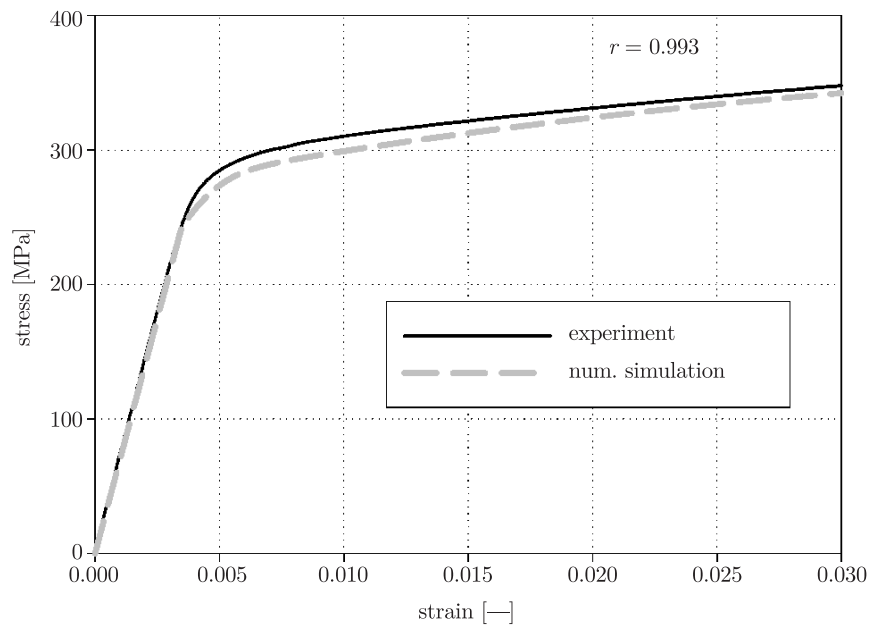for the specimen cut across the rolling direction of the sheet

Figure 9. Results of B-P simulation of the uniaxial tension test for $\dot{\varepsilon} = 1 \cdot 10^{-2} \, \mathrm{s}^{-1}$, for the specimen cut across the rolling direction of the sheet

Figure 10. Results of B-P simulation of the uniaxial tension test for $\dot{\varepsilon} = 1 \cdot 10^{-4} \, \mathrm{s}^{-1}$, for the specimen cut along the rolling direction of the sheet

Figure 11. Results of B-P simulation of the uniaxial tension test for $\dot{\varepsilon} = 5 \cdot 10^{-4} \mathrm{s}^{-1}$, for the specimen cut along the rolling direction of the sheet

Figure 12. Results of B-P simulation of the uniaxial tension test for $\dot{\varepsilon} = 1 \cdot 10^{-3} \mathrm{s}^{-1}$, for the specimen along the rolling direction of the sheet
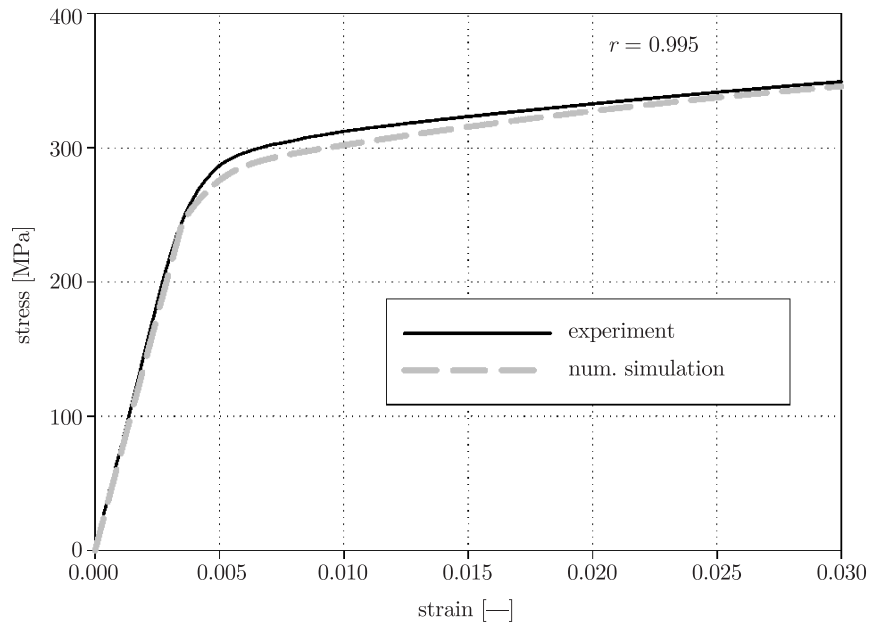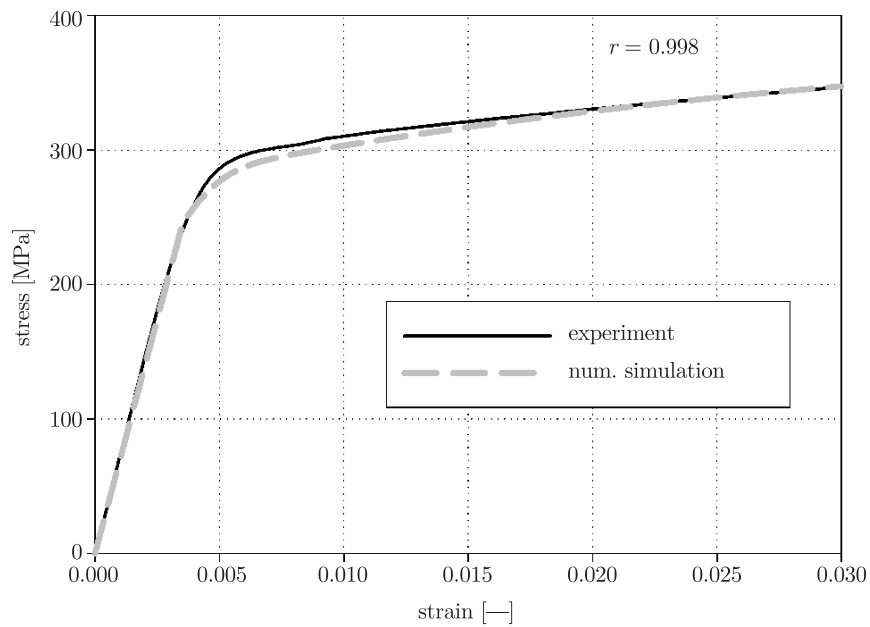
Figure 13. Results of B-P simulation of the uniaxial tension test for $\dot{\varepsilon} = 5 \cdot 10^{-3} \, \text{s}^{-1}$, for the specimen cut along the rolling direction of the sheet

Figure 14. Results of B-P simulation of the uniaxial tension test for $\dot{\varepsilon} = 1 \cdot 10^{-2} \, \text{s}^{-1}$, for the specimen cut along the rolling direction of the sheet
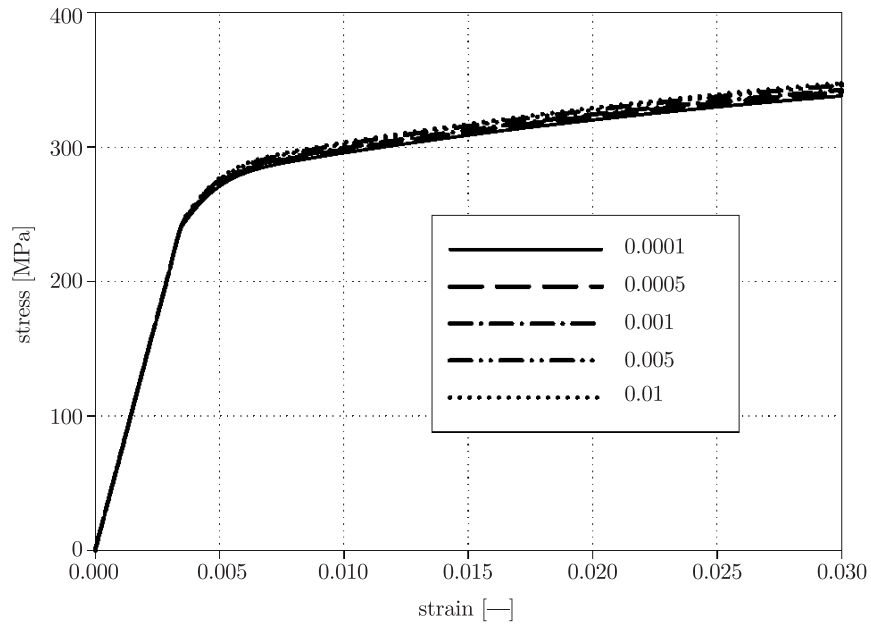
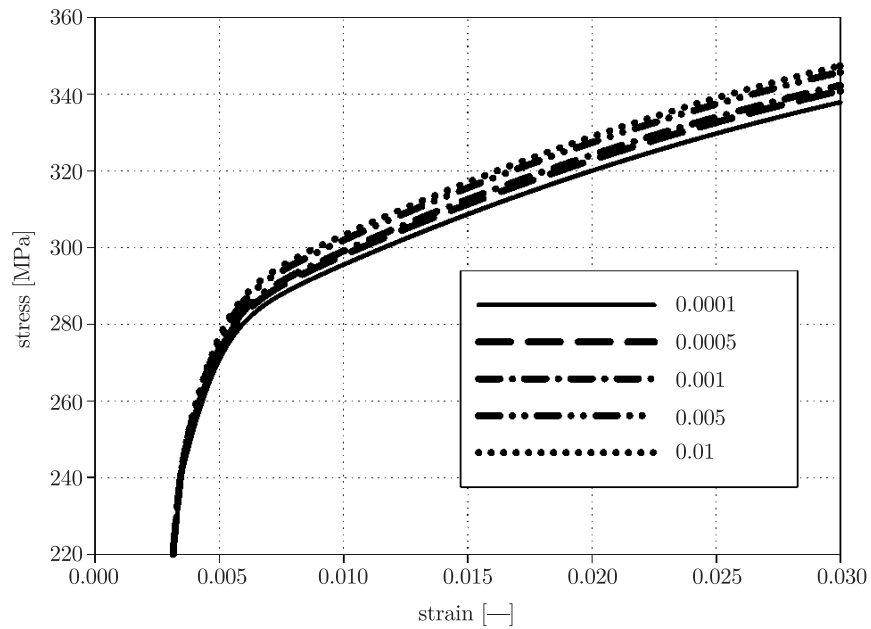**Figure 15.** Results of B-P numerical simulation of the uniaxial tension test

Figure 16. Results of B-P numerical simulation of the uniaxial tension test, inelastic range
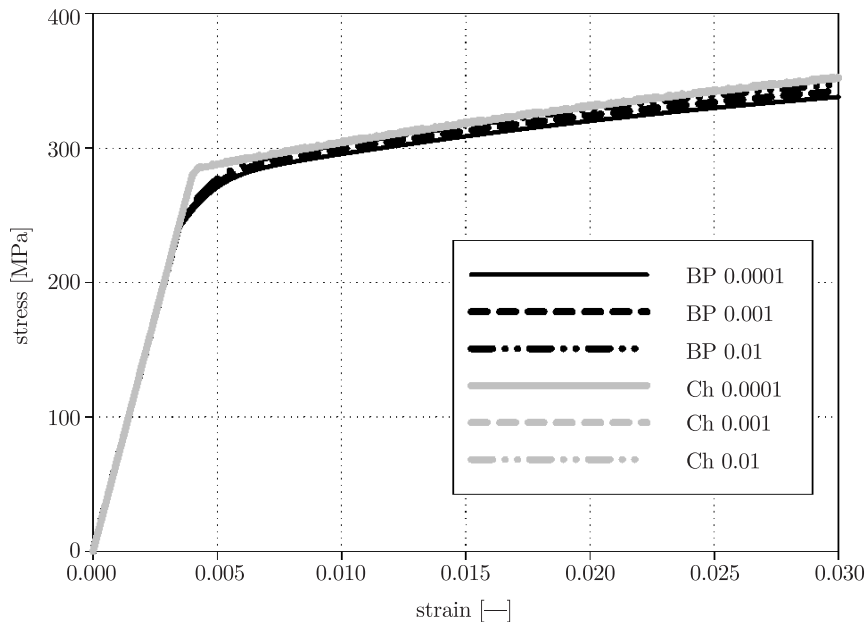
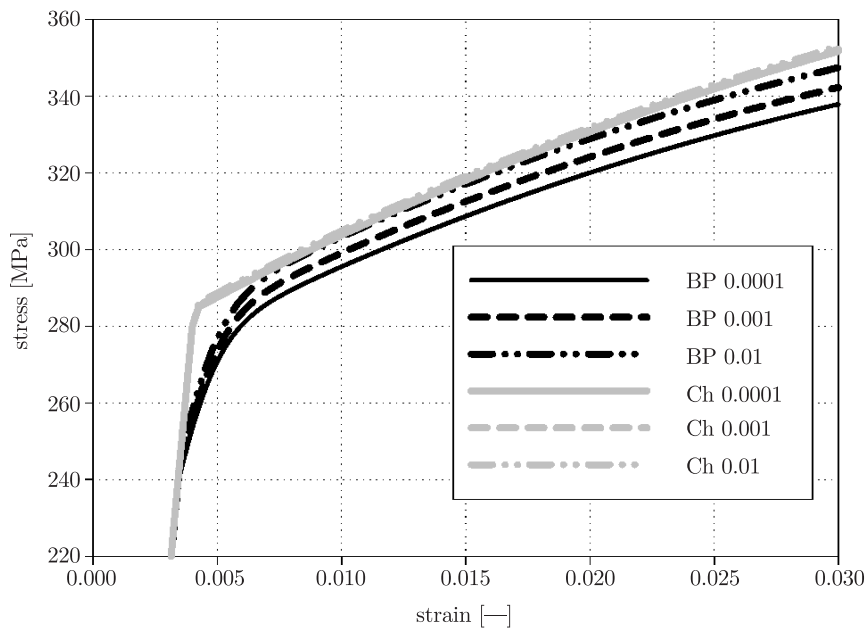**Figure 17.** Results of B-P and Chaboche numerical simulations of uniaxial tension tests

Figure 18. Results of B-P and Chaboche numerical simulations of uniaxial tension tests, inelastic range

Table 6. Parameters of the elasto-viscoplastic Chaboche model for AA2017 aluminium alloy

E [MPa]	k [MPa]	b [—]	R_1 [MPa]	a [MPa]	c [—]	n [—]	K [vMPa]
70 000	282.3	19.6	115.2	1464.7	41.3	10.0	5.0

Numerical simulations of uniaxial tensile tests the with Chaboche model performed for three different constant strain rates were compared with the results obtained with the Bodner-Partom model (see Figures 17 and 18).

7. Conclusions and final remarks

The identification of the elasto-viscoplastic Bodner-Partom model was successfully performed. For the description of the AA2017 alloy behaviour the uniaxial tension tests were used. Good agreement was observed between the stress-strain relations obtained from laboratory tests and from numerical simulations.

The obtained results encouraged us to continue this line of research employing further experimental data (*e.g.* biaxial tension tests). In our further investigations, we propose to focus on the effects of the rolling direction on material properties values and on the application of the anisotropic model.

References

[1] Kardas D, Kluger K, Ładoga T and Ogonowski P 2008 *Material Science* **4** 541

[2] Ramberg W and Osgood W R 1943 *NACA Technical Note* **902**

[3] Kuruppu M D, Williams J F, Bridgford N, Jones R and Stouffer D C 1992 *J. Strain Anal. Eng. Des.* **27** 85

[4] Kowalewski Z L, Hayhurst D R and Dyson B F 1994 *J. Strain Anal. Eng. Des.* **29** 309

[5] Gelin J-C and Ghouati O 1998 *Commun. Numer. Methods Eng.* **12** 162

[6] Santhanam S 2000 *J. Mat. Sci.* **35** 3647

[7] Zhao K M and Lee J K 2001 *J. Eng. Mat. and Tech.* **123** 287

[8] Lauro F, Bennani B, Croix P and Oudin J 2001 *J. Mater. Process. Technol.* **118** 472

[9] Omerspahic E, Mattiasson K and Enquist B 2006 *Int. J. Mech. Sci.* **48** 1525

[10] Martínez H V, Coupard D and Girot F 2006 *J. Mater. Process. Technol.* **173** 252

[11] Diot S, Guines D, Gavrus A and Rageau E 2006 *Int. J. Forming Processes* **9** 167

[12] Omerspahic E 2007 *J. Mech. Eng. Sci.* **221** 971

[13] Majak J, Toompalu S and Pohlak M 2008 *J. Ach. Mat. and Man. Eng.* **27** 63

[14] Chaparro B M, Thuillier S, Menezez L F, Manach P Y and Fernandes J V 2008 *Comp. Materials Science* **44** 339

[15] Bouffioux C, Eyckens P, Henrard C, Aerens R, Van Bael A, Sol H, Duflou J R and Habraken A M 2008 *Int. J. Material Forming* **1** 1147

[16] Zhang C, Leotoing L, Guines D and Ragneau E 2009 *J. Mater. Process. Technol.* **209** 3849

[17] Bodner S R and Partom Y 1975 *J. Appl. Mech.* **42** 385

[18] Kłosowski P and Woznica K 2007 *Elasto-viscoplastic Non-linear Constitutive Models in Selected Applications of Structures Analysis*, Wydawnictwo Politechniki Gdanskiej, Gdansk (in Polish)

[19] Marquardt D W 1963 *J. Soc. Industrial and Appl. Math.* **11** 431

[20] Woznica K and Kłosowski P 2000 *Arch. Appl. Mech.* **70** 561

[21] Kłosowski P, Pyrzowski Ł and Woznica K 2008 *Machines Dynamics Problems* **32** 44

[22] Chaboche J L 1989 *Int. J. Plasticity* **5** 247